

Role of the Solvation Shell Structure and Dynamics on K-Ion and Li-Ion Transport in Mixed Carbonate Electrolytes

Jassiel R. Rodriguez,^{*[a]} Bumjoon Seo,^{*[a]} Brett M. Savoie,^[a] and Vilas G. Pol^[a]

Ethylene and diethyl carbonates (EC:DEC) have been attractive solvents for Li-ion electrolytes because these can exhibit a good ionic conductivity and stable electrochemical performance. However, in the contemporary K-ion electrolytes, KPF_6 presents a limited solubility of $\sim 0.6 \text{ M}$ in EC:DEC (volume ratio 1:1), which restricts its performance. Here, the molecular basis for these distinct solvation behaviors is clarified by combining experimental attenuated total reflectance-infrared spectroscopy and electrochemical impedance spectroscopy measurements

with molecular dynamics simulations, revealing the distinct roles of EC and DEC solvents on the solubility, ionic conductivity, and solvation shell structures of KPF_6 and LiPF_6 salts in EC:DEC mixtures. In turn, these insights have enabled the formulation of a new K-ion electrolyte with EC:DEC volume ratio of 1.5 that exhibits significantly increased KPF_6 solubility ($\sim 0.9 \text{ M}$) and ionic conductivity, reaching 13.99 mS cm^{-1} at 25°C .

1. Introduction

Although Lithium ion batteries (LIBs) have continuously increased their performance, energy storage and sales since their arrival to the secondary battery market in 1991,^[1] large-scale energy storage applications require post-Li technologies based on earth abundant materials.^[2–5] As an ascendant post-Li candidate, batteries based on potassium-ion redox couples (KIB) present several attractive features including a low standard reduction potential (-2.93 V vs. SHE), a small Stokes radius (3.6 Å for K-ions), and abundant natural availability.^[4–6] As with every emergent technology,^[7] the development of KIBs is facing some important challenges to achieve viability, such as the development of negative and positive potassium intercalation electrodes with long-life cycle performance,^[8–15] and the design of novel electrolytes for the stable operation of the KIBs.^[16,17] Although it is well known that a commercial KIBs will need an optimized electrolyte,^[17] only limited efforts have been made to develop tailored electrolytes.^[18–21] In particular, most published KIB electrolytes have been based directly on Li-ion electrolytes without addressing the fundamental differences in the solvation behaviors of these cations.^[18] Recent work has highlighted many aspects of KIB electrolytes that indicate substantially different behavior from Li-ion electrolytes, including distinct solid electrolyte interphase formation behaviors,^[22] shifted voltage and temperature stability windows,^[23] and distinct intercalation dynamics.^[23] Despite these manifold differences, the molecular details of K-ion solvation in typical carbonate solvents remains unexamined

and undermines the development of electrolyte design rules optimized for KIBs.^[24]

Prevailing KIB electrolytes are based on KPF_6 dissolved in a mixture of ethylene carbonate (EC) and diethyl carbonate (DEC).^[25] In analogy with Li-ion electrolytes, carbonates are thought to be promising KIB solvents due to their high dielectric constant, which promotes ion dissociation, and decomposition into stable solid electrolyte interphases on common electrodes.^[26] However, the limited solubility of KPF_6 salt in linear carbonates, DEC, ultimately restricts the conductivity of contemporary KIB electrolyte, $\sim 0.6 \text{ M}$ KPF_6 in EC:DEC (volume ratio 1:1).^[25] The molecular basis for these distinct solvation behaviors is interrogated here using a combined experimental and theoretical approach. Experimental ATR-FTIR and EIS measurements are combined with molecular dynamics (MD) simulations to elucidate the solvation shell structures of KPF_6 and LiPF_6 salts in EC:DEC solvent mixtures. This comparative study reveals the distinct roles played by cyclic carbonates in promoting the solubility of KPF_6 and linear carbonates in suppressing electrolyte viscosity. In turn, these insights have allowed us to formulate a K-ion electrolyte, 0.9 M KPF_6 in EC:DEC (volume ratio 1.5:1) with the highest KPF_6 salt loading and conductivity reported to date for this mixture of solvents.

2. Results and Discussion

To increase the KPF_6 salt solubility in the EC:DEC solution, and improve its ionic conductivity, there are some fundamental aspects in the solvation shell-structure of K-ion in the solution that must be revealed. Although the dipolar moment of EC and DEC molecules play a key role on the solvation of both KPF_6 and LiPF_6 salts, there is a lack of information about the changes on EC and DEC active FT-IR vibration, which are related to their dipolar moments in EC:DEC solutions. It can be monitored via FT-IR to understand in depth the evolution of the ion-dipole

[a] Dr. J. R. Rodriguez, Dr. B. Seo, Dr. B. M. Savoie, Dr. V. G. Pol
Davidson School of Chemical Engineering
Purdue University
480 Stadium Mall Drive, West Lafayette, IN 47907, USA
E-mail: rodrig571@purdue.edu
seo89@purdue.edu

 Supporting information for this article is available on the WWW under
<https://doi.org/10.1002/batt.202100223>

interaction between KPF_6 or LiPF_6 salts in a mixture of EC and DEC solvents. Multiple FT-IR spectra were recorded from EC:DEC solutions at different EC concentrations to reveal the existence of any change in C–O and C=O vibrations. Figure 1 shows the normalized FT-IR spectra at different wavenumber regions that reveals an interesting change in the active vibration of DEC as EC concentration increases. In the 650 cm^{-1} to 1000 cm^{-1} region (Figure 1a), DEC present three strong peak at 791 cm^{-1} , 853 cm^{-1} and 980 cm^{-1} ascribed to O–CO–O rocking, $-\text{CH}_2-$ out of the plane rocking (or O–CO–O out of the plane bending) and O–CO–O or C–O–C symmetric stretching at DEC molecule,^[27] respectively. As the concentration of EC increase in the solution the intensity of EC active vibrations arises at 715 cm^{-1} (O–C–O rocking), 772 cm^{-1} ($-\text{CH}_2-$ and O–CO–O rocking) and 969 cm^{-1} (O–CO–O and C–O–C symmetric stretching).^[27] Also, two small peaks at 900 cm^{-1} and 893 cm^{-1} are present that are ascribed to O–C–O bending and $-\text{CH}_2-$ wagging vibrations in DEC and EC molecules,^[27] respectively. Figure 1(b) shows that the C–O vibration in the EC molecule exhibits a red shift from 1072 cm^{-1} to 1065 cm^{-1} , which could be due to an elongation of the C–O bond. Meanwhile, the C–O vibration in DEC exhibits a blue shift from 1246 cm^{-1} to 1258 cm^{-1} as the concentration of EC increases in the solution (Figure 1c), which could be due to a contraction of the bond or changes on the environment of the molecule. In contrast, the C=O vibration in the DEC molecule remains constant at 1740 cm^{-1} as the EC concentration arises^[28] (Figure 1d), while the C=O vibration in EC exhibits a red shift from 1808 cm^{-1} to 1796 cm^{-1} ,^[28] which could be due to an

elongation of its C=O bond in the solution that could increase its dipolar moment, and then, its ability to interact more effectively with alkaline ions via an ion-dipole interaction. Interestingly, as the EC concentration increases in the solution, a new peak appears at $\sim 1772\text{ cm}^{-1}$ that is attributed to a Fermi resonance.^[28] The ration of this peak vary with respect to C=O peak intensity, then the intensity attributed to the Fermi resonance peak could be more related to: i) an overlapping between the carbonyl vibrations at EC and DEC molecules; or ii) the dipolar moment of the EC molecule increases in the EC:DEC solution.

After revealing the different changes on some of the active vibration modes in EC and DEC molecules in the EC:DEC mixture, the relationship between the alkaline ion-dipole interactions or their cation coordination sphere and the Li- and K-ion conductivity in the electrolytes can be revealed and understood in depth. Li-ion electrolytes with a LiPF_6 concentration of 1.0 M in an EC:DEC solution (volume ratio 1:1) exhibits high ionic conductivity and good performance in battery applications.^[29,30] As EC exhibits higher dielectric constant than DEC, it is expected that the solubility of KPF_6 or LiPF_6 salts increases in EC:DEC mixtures. However, EC is solid at 25°C (optimum temperature for Li-ion battery operation), leading to the utilization of an optimum amount of EC in the mixture).^[29,30] An electrolyte with a LiPF_6 concentration of 1.0 M can be easily prepared in a solution of EC:DEC ratio 1:1, however this is not the case for KPF_6 that exhibits a low solubility in EC:DEC (ratio 1:1) of 0.7 M, leading to precipitation of KPF_6 .^[25] To reveal the ion-dipole interactions between KPF_6

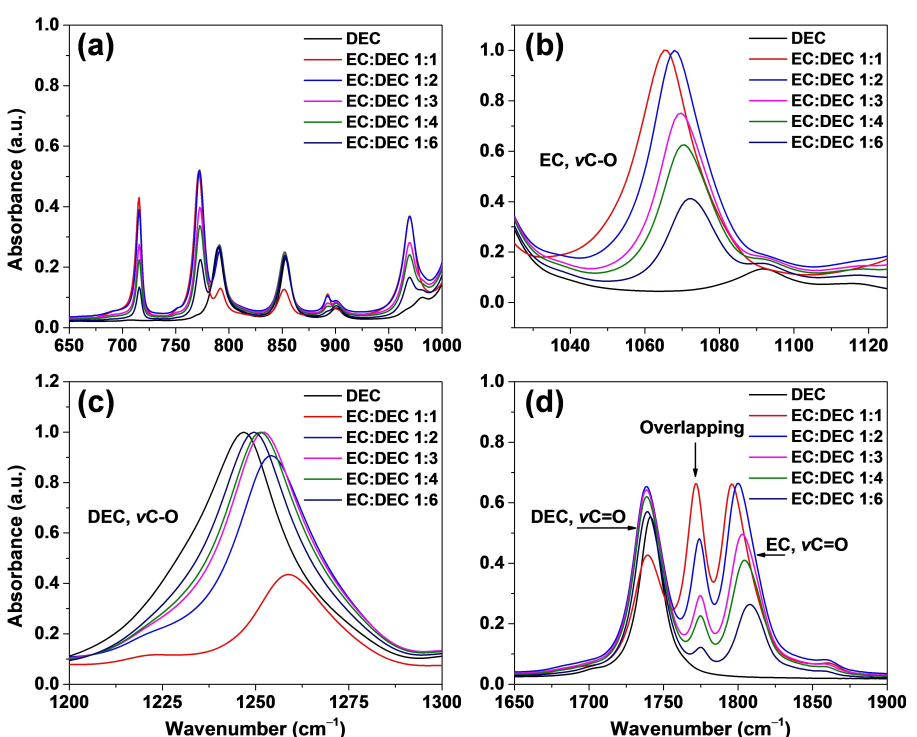


Figure 1. FT-IR spectra of the prepared EC:DEC solutions at room temperature at different wavenumber ranges: a) Skeletal bending mode region, C–O vibration in b) EC and c) DEC molecules, and d) C=O region.

or LiPF₆ salts in EC:DEC ratio 1:1, FT-IR spectra were recorded at different concentration of salts (0.2, 0.4, 0.6 and 0.8 M), as shown in Figure 2. The DEC and EC vibration modes in the skeletal region (low wavenumber from 650 to 1000 cm⁻¹, see Figure 2a,b) are not shifted by the addition of the alkaline salts, however, their intensities increase and hence their dipolar moments increase, which is more significant for the DEC vibrational modes (i.e., the 791 cm⁻¹, O—CO—O rocking and 900 cm⁻¹, O—C—O bending) for the LiPF₆ case. For both cases, the IR peak at 969 cm⁻¹ ascribed to O—CO—O and C—O—C symmetric stretching exhibiting an intensity reduction as a new vibrational mode appears at 741 cm⁻¹ that is related to O—C—O and C—O—C deformations.

The IR peak related to P—F stretching arises at 839 cm⁻¹ as the alkaline salt concentration increases in the EC:DEC mixture.^[31] This peak is followed by a small shoulder around 877 cm⁻¹ that indicates a high anisotropic environment for [PF₆]⁻ anion in both cases, as a result of the formation of contact ion pairs or aggregates (Figure 2a,b).

Within the C—O region (LiPF₆ case), both DEC and EC molecules exhibit a strong IR vibration at around 1259 and 1068 cm⁻¹ that are attributed to C—O vibration, see Figure 2(c,e). Also, an additional new IR active band arises at 1300 and 1085 cm⁻¹. The intensities of these new peaks are strongly sensitive to salt concentration, and their spectral signature is characteristic of contact ion pairs and aggregates of LiPF₆.^[32] Interestingly, for the KPF₆ case, the C—O vibration of DEC exhibits two changes (see Figure 2f): i) Its intensity increases with the addition of salt, reaching the highest dipolar moment at 0.6 M that is almost the highest solubility of KPF₆ in EC:DEC ratio 50:50; and ii) the appearance of a small IR band at 1300 cm⁻¹ ascribed to the formation of contact ion pairs and aggregates. The C—O vibration of EC presents a positive shift of 3 cm⁻¹ (Figure 2d), which could be due to a change in its chemical environment as KPF₆ concentration increases.

Within the carbonyl region (LiPF₆ case, Figure 2g), the IR peak position ascribed to DEC molecule is unchanged, although its width increases as result of a peak overlapping between C=O at free-DEC molecules (1742 cm⁻¹) and C=O at Li⁺-DEC interaction (1715 cm⁻¹), because last one modifies the C=O stretching energy.^[33] Interestingly, as the solubility test demonstrates, DEC molecules are less susceptible to dissolve the KPF₆ salt (< 0.2 M in DEC) and form a K-carbonyl interaction. In the KPF₆ case (Figure 2h), the carbonyl vibration from DEC suffers a negative shift of 1 cm⁻¹ to low wavenumber and an enlargement of its dipolar moment, meanwhile the intensity of the carbonyl vibration at EC molecules moderately decay, which could be due to the formation of K-EC interactions that generate a reduction of intensity on the overlapping peak at 1772 cm⁻¹. The solvation of KPF₆ salt depends on the EC concentration in an EC:DEC solution as EC dielectric constant is higher than that one of DEC.^[34]

Through the deconvolution of the carbonyl vibrations at different KPF₆ and LiPF₆ concentrations, it is possible to assign the effective contribution of alkaline ion-EC and -DEC interactions to the IR spectra,^[35] as shown in Figure 3(a,b). At low concentrations of LiPF₆ in the mixture of solvents, 0.2 M, the EC solvent interacts mainly with the Li ion (Figure S1). Around 21% of the EC molecules generates an ion-dipole interaction while around of 8% DEC molecules interacts with Li-ions. Interestingly, as LiPF₆ concentration increases until 0.8 M, Li-EC interaction does not increase significantly, remaining around 22% (Figure S1). However, the Li-DEC interaction increases until reaching around 32% of the DEC molecules, which indicates the key role of the DEC solvent on dissolving the Li salt. In contrast, KPF₆ salt is mainly dissolved by EC molecules because 16% of the EC molecules form an ion-dipole interaction at 0.2 M (Figure S2), which increases until 20% at 0.8 M. Meanwhile, K-ions interact with 3% and 7% of the DEC molecules at 0.2 and 0.8 M, respectively. Also, Figure 3(c) shows that at low alkaline salt concentrations (0.2 M), in both cases the EC

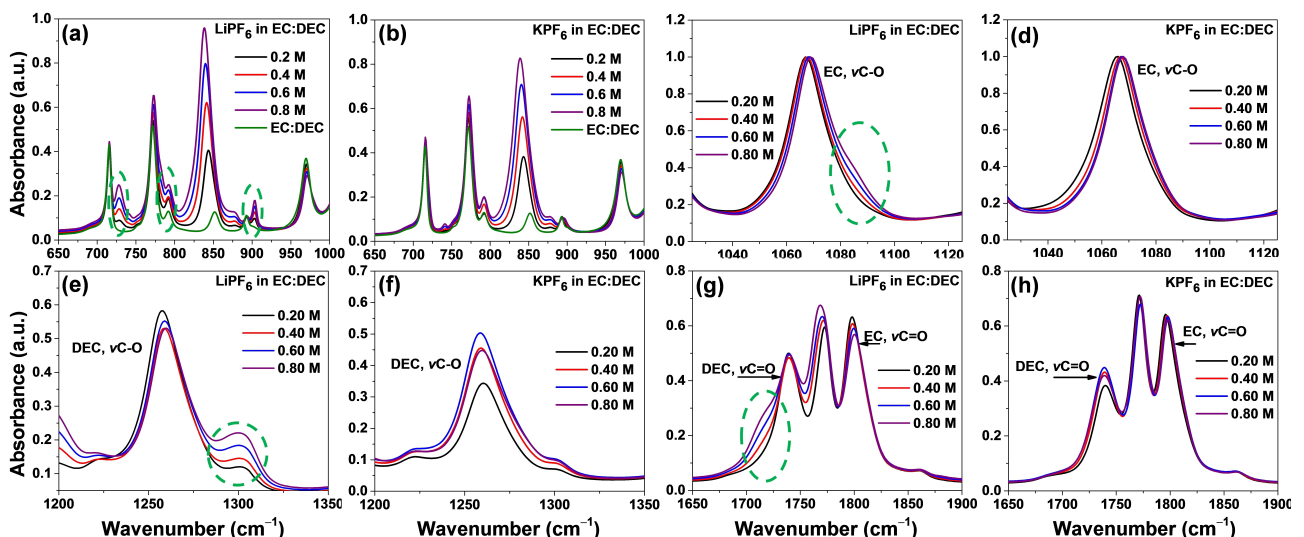


Figure 2. FT-IR spectra of LiPF₆ (a,c,e,g) and KPF₆ (b,d,f,h) in EC:DEC (volume ratio 1:1) at different concentrations.

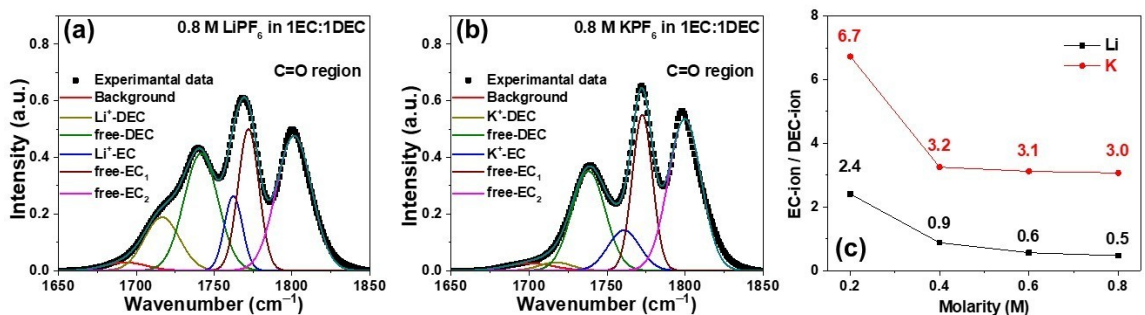


Figure 3. IR spectra of the C=O stretching vibrations deconvolution at 0.8 M alkaline salt in EC:DEC (ratio 1:1): a) LiPF₆; b) KPF₆; and c) ion-carbonate interaction ration at different molar concentrations.

molecules coordinate principally with the alkaline ions, however, at high LiPF₆ concentrations around one Li-EC complex is created by each two Li-DEC interactions. However, at high KPF₆ concentrations around of 3 K-EC interactions are originated by each one of K-DEC, revealing that the KPF₆ and LiPF₆ salts follow different dissolution trends in the EC:DEC mixture, and therefore, both salts present different saturation points and transport mechanisms in the electrolyte. To prove the supposition that the solubility of KPF₆ in the EC:DEC mixture depends mainly on the EC concentration, a mixture of EC:DEC ratio 1.5:1 (or 3:2) was prepared. Remarkably, such EC:DEC solution reaches its saturation point (maximum solubility) at 0.9 M KPF₆ being completely transparent (See Figure 4a), which has not been achieved previously for this type of electrolyte. In contrast, the electrolyte at 1.0 M KPF₆ in EC:DEC (volume ratio 1.5EC:1DEC) displays a cloudy color, indicating the precipitation of the KPF₆ salt. The FT-IR spectrum at carbonyl region from the new formulated electrolyte, 0.9 M KPF₆ in 1.5EC:1DEC, revealed similar behavior to the EC:DEC ratio 1:1 (Figure 4b). In which, the addition of KPF₆ salt promotes a slight broadness in the C=O vibration of the DEC molecule at 1740 cm⁻¹ as K-

DEC interactions appears at 1717 cm⁻¹, and also, a loss of intensity is observed on the C=O vibration of the EC molecule at 1799 cm⁻¹ caused by the appearance of a peak at 1762 cm⁻¹ related to K-EC interactions. The deconvolution of the carbonyl vibrations at 0.9 M KPF₆ in 1.5EC:1DEC shows the contribution of K-EC and K-DEC interactions (Figure 4c). For this case, around 20% of the EC molecules interact effectively with K-ions, while around of 7% DEC molecules form an ion dipole interaction with K-ions, demonstrating that the KPF₆ can be effectively dissolved in a mixture of organic carbonates with a high concentration of EC.

The solvation behaviors of Li⁺ and K⁺ ions are further investigated at the molecular level using MD simulations. The ion-solvent interactions are clearly differentiated in the limits of the two solvents EC and DEC, while the interactions in the mixture are also important for the comparison with the experiments. Therefore, baseline differences in ion coordination for the pairs of ion and solvent were established for the 1:0, 1:1, and 0:1 EC:DEC cases based on the radial distribution function. The radial distribution function characterizes the local structure of a fluid and its deviation from the unity indicates

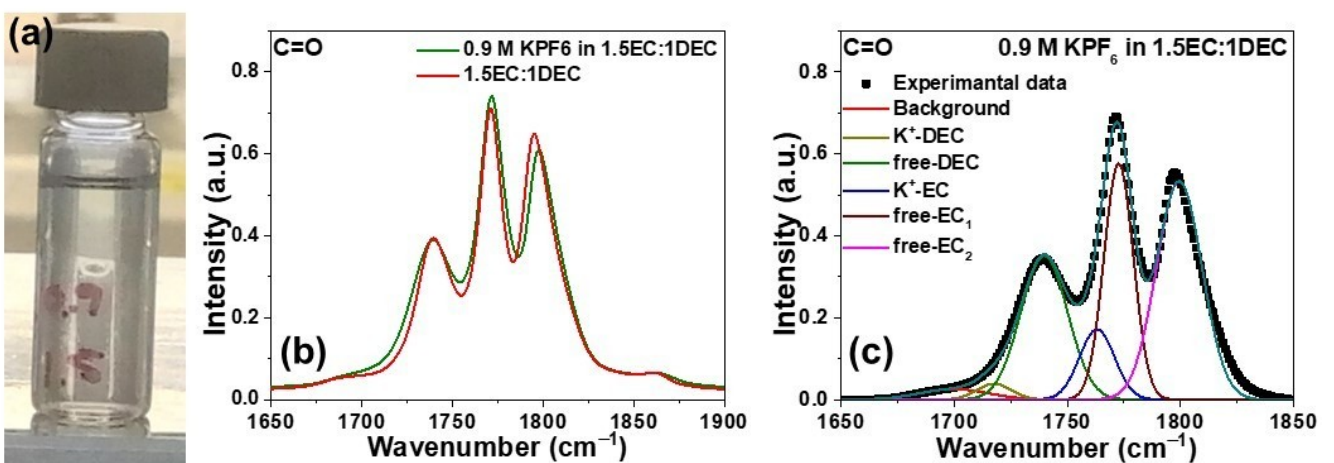


Figure 4. Information of the transparent 0.9 M KPF₆ in EC:DEC (ratio 1.5:1) electrolyte: a) Photo of the electrolyte; b) FT-IR spectra at carbonyl region; and c) the deconvolution of the C=O vibrations.

correlations between the associated particles.^[36] The radial distribution functions in Figure 5 between both cations and the carbonyl oxygens show a large peak at the first solvation shell in all cases, indicating the key role of this moiety in solvating both cations. However, the radial distribution function between the cations and the anions (indicated by the phosphorus atom P) show distinct behaviors. In pure EC, the cations are coordinated with the solvent molecules (Figure 5a) while having less interaction with the anions, which results in no observable peak in the first solvation shell (Figure 5b). In the pure DEC case, however, the cations are strongly coordinated with the anion indicated by the high peak intensity of radial distribution function between the cations and the phosphorus atoms (Figure 5f). As for the EC:DEC (ratio 1:1) mixture, the coordination between the cation and anion can be considered similar to that of the pure EC case (Figure 5d), showing small degrees of coordination but with much less intensity in comparison with pure DEC. To demonstrate the differential solvation behaviors of EC and DEC, we compared the separate radial distribution functions for the carbonyl groups belonging

to the different solvent moieties in the mixture. A comparison between that of the carbonyl groups in EC and DEC molecules shows that the peaks for the EC molecules (Figure 6a) are five times higher than that for the DEC molecules (Figure 6b), which demonstrates that EC is the major component of the cation solvation structure when present, consistent with experiments. The distinct solvation behaviors between the solvents shown by the radial distribution functions also indicate that strong cation-anion interactions outcompete solvation in DEC. On the other hand, the absence of this strong interaction in pure EC and EC:DEC mixture reflects the experimental observation of suppressed salt precipitation in these solvents, whereas in pure DEC this interaction is strong enough to cause the salt precipitation.

The radial distribution functions showed that the solvation behaviors of the cations are different in the solvents. The most distinguishing feature was the existence of strong cation-anion interaction in the pure DEC. The representative solvation structures from trajectory snapshots in Figure 7 reveal the molecular basis for this interaction. In pure EC, the ions are

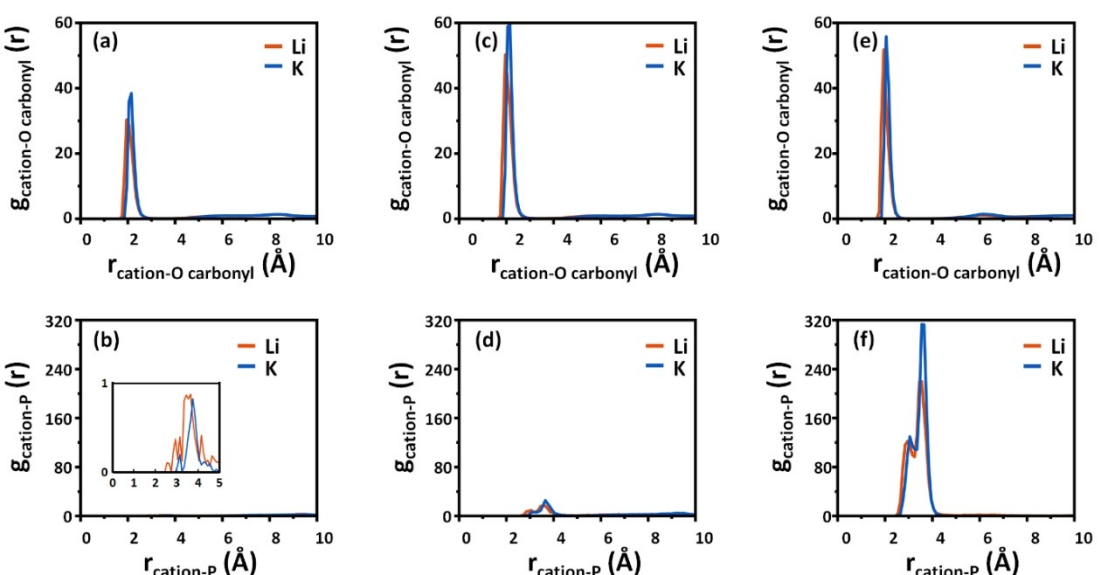


Figure 5. Radial distribution functions for the Li- and K-ions. The upper panel shows the radial distribution functions between the cation and the oxygen atom of the carbonyl group of the solvents whereas the lower panel shows that between the cation and the phosphorus atom of the anions. The investigated solvents are a,b) pure EC, c,d) EC:DEC (ratio 1:1), and e,f) pure DEC.

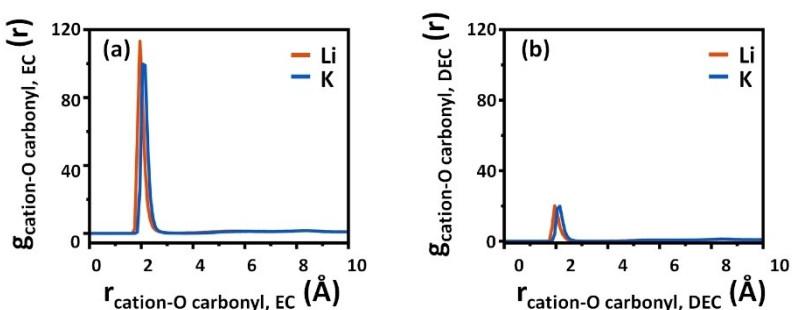


Figure 6. Radial distribution functions for the Li- and K-ions in the EC:DEC (ratio 1:1) mixture. The radial distribution functions between the cation and the oxygen atom of the carbonyl group for the a) EC and b) DEC molecules.

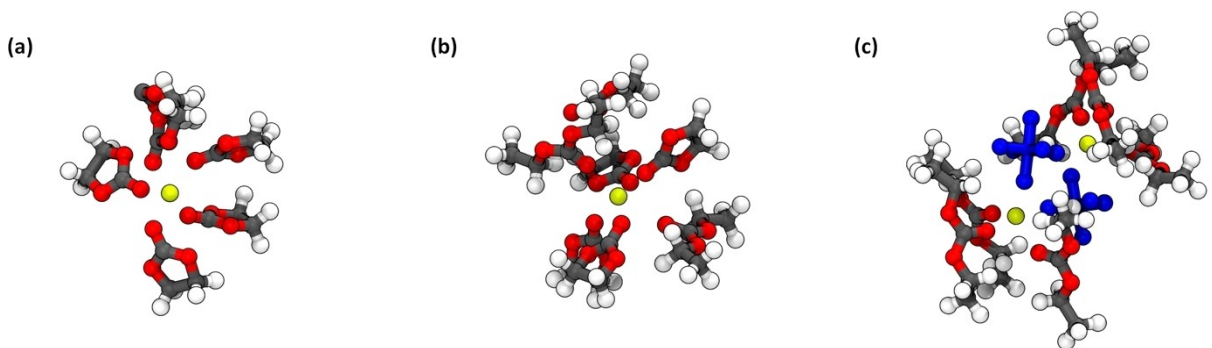


Figure 7. Snapshots from the MD simulations of different systems showing typical coordination of K-ions in the different solvent environments. a) Pure EC, b) EC:DEC (ratio 1:1), and c) pure DEC. In the pure EC and the mixture case, the K-ions are mainly coordinated by the oxygen atoms of the carbonyl group of the EC molecules. As for the pure DEC case, the K-ions are still partly coordinated by the oxygen atoms of the carbonyl group of the DEC molecules, but the stronger interactions between cations and the anions inhibit the solvation of the ions.

highly coordinated by the oxygen atoms of the carbonyl group of the EC molecules. On the other hand, in the pure DEC case, the K-ions are coordinated by the oxygen atoms of the carbonyl group of the DEC molecules to some extent as the ions are surrounded by the DEC solvent. However, the interactions between the K-ions and PF_6^- -ions are not broken throughout the whole trajectory, thereby explaining the high peak in the radial distribution functions between the cation and the anion in the DEC solvent case. Lastly, in EC:DEC (ratio 1:1) mixture, the K-ions are mainly coordinated by the oxygen atom of the carbonyl group of EC molecules as they were in the pure EC case. This EC-dominated solvation structure in the mixture confirms the role of EC in the mixture and explains the absence of strong interaction between anions and cations in pure DEC which is obscured by EC molecules when they are present.

Further MD simulations were performed for the K-ions and mixture systems where the radial distribution functions were calculated to investigate the effects of both solute and solvent concentrations of the mixtures. As with the previous case of pure solvents, similar radial distribution functions between the K-ions and oxygen atoms of the carbonyl groups are shown in Figure 8(a). A slight decrease in the ion-oxygen peak is observed as the concentration of the ion concentrations are increased, which indicates minor speciation. As for the radial

distribution functions between the cations and phosphorus atom on the anions, more complex trends are observed. The trends are understandable, however, when compared with the experimental evidence. As the solute concentrations reach closer to the expected cloud point in EC:DEC (ratio 1:1) mixtures, the interaction at the closer range between the cations and anions increase up to precipitation as in Figure 8(b and c) with the respective solvents of EC:DEC (ratio 1:1) and EC:DEC (ratio 1.5:1). When the EC concentration is increased as in Figure 8(c), however, the interactions are decreased as more coordination between the K-ion and oxygen atoms of the carbonyl group of EC occur, as suggested from the experiments on the larger solubility of KPF_6 in the mixture with increasing EC concentration. To quantify the distinct solvation behaviors of Li-ion and K-ion in EC and DEC mixtures, we also performed thermodynamic integration simulations to calculate the solvation free energies associated with inserting the ions into the respective solvents. The larger decrease in the solvation free energy with the insertion of a cation is closely related to the better solubilization of the ion in the solvent. In Figure 9, the solvation free energies are compared for the pairs of ion and solvent. For both ions, insertion into EC results in a lower solvation free energy which supports the notion that EC drives the solvation of the ions. Furthermore, similar to the previous properties that were analyzed, insertion into the EC:DEC (ratio

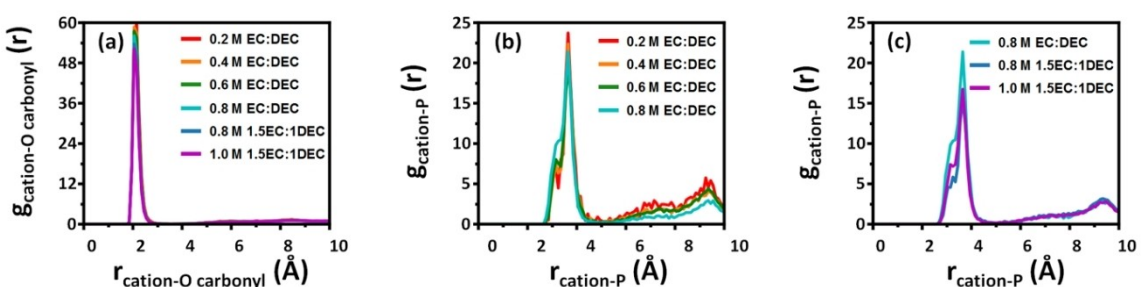


Figure 8. Radial distribution functions for the cation (K-ion) in mixtures of EC and DEC with varying solute and solvent concentrations. a) Radial distribution functions between K-ions and the oxygen atom of the carbonyl group of solvent molecules. b) Radial distribution functions between K-ions and the phosphorus atom of the anion in EC:DEC (ratio 1:1) mixtures with varying solute concentrations. c) Radial distribution functions between K-ions and the phosphorus atom of the anion in EC:DEC mixture with varying solvent ratios and solute concentrations.

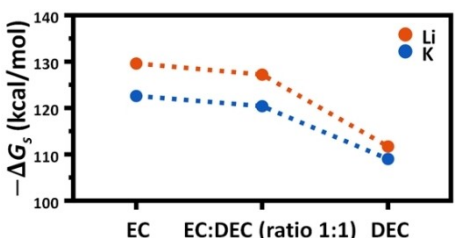


Figure 9. Solvation free energies for Li- and K-ions in pure solvents and EC:DEC (ratio 1:1) mixture obtained from the insertion of a single cation into the solvents with the thermodynamic integration method.

1:1) mixture show free energy values that are comparable to EC-only, which suggests that the solvation behavior is still dominated by the EC component of the solvent mixture. In contrast, the solvation free energies of both ions are strongly suppressed in DEC. Notably, the higher overall solvation free energies for Li-ion in EC and EC:DEC, may explain the reduced sensitivity of Li-ion electrolytes to the solvent composition, whereas for K-ion electrolytes tuning the EC concentration is critical to achieve appreciable KPF_6 solubility.

To understand the evolution of the alkaline ion transport properties in EC:DEC as the KPF_6 and LiPF_6 concentration arise in the electrolyte, multiple electrochemical impedance spectroscopy was carried out at different temperatures to calculate their ionic conductivities (σ) and activation energies (E_a)^[37,38] (see Figures S3–S5). The impedance of each electrolyte system decreases as the testing temperature increase from 25 °C to 60 °C (see Figure 10a), these values were obtained via an electric equivalent circuit fitting using a Randles circuit. Also, as the salt concentration increases in both potassium and lithium systems, the ionic conductivity of the electrolytes rises in general (Figure 10b and S6). Lithium electrolytes present higher ionic conductivities than potassium ones at the same concentration, which could be related to their small activation energies, see Table S1. Among the potassium electrolytes, 0.9 M KPF_6 in EC:DEC ratio=1.5 presents the highest value of ionic conductivity (13.99 mScm^{-1}) at 25 °C, exhibiting the lowest activation energy for K-ions (20.1 kJmol^{-1}) which is close to lithium electrolytes. It demonstrates that a high concentration of EC solvent in the electrolyte can effectively dissolves

a large amount of KPF_6 salt, improving its ionic conductivity in agreement with the IR data. Also, it is noteworthy that there is a super-linear increase in the conductivity with respect to the salt concentration when it is increased from the most dilute salt compositions. This nonlinearity could be attributed to ion specification with respect to concentration which can increase the activity of the K-ion non-linearity, where further investigation will be worthy for determining the speciation dynamics.

3. Conclusion

The IR analysis of different EC and DEC active vibrations in both potassium and lithium electrolytes, allowed a better understanding of the ion-dipole interaction by the coordination between K-ion or Li-ion with EC and DEC solvents as well as their role on the electrolyte ion conductivity at different salt concentrations and temperatures. For potassium electrolytes, the EC molecule plays a major role on the solubility and solvation of KPF_6 and K-ion, respectively. While, for lithium electrolytes, DEC coordinates with lithium as its concentration increases in the electrolytes. Comparison of the radial distribution functions calculated from the MD simulation trajectories of different solvent environments showed that salt speciation is suppressed in both pure EC and EC:DEC formulations in comparison with DEC. In particular, the mixed formulation still exhibits a solvation structure dominated by EC, while the DEC component mainly serves to reduce the electrolyte viscosity and suppress the freezing point. These findings, along with the ion-specific solvation free energy calculations, revealed the underlying role of EC molecules in enhancing the solvation of the ions, leading to the better formulation suggested in the present work. Therefore, the new potassium electrolyte formulation with EC:DEC ratio=1.5, enables a significantly increased KPF_6 solubility (~0.9 M) without potassium salt precipitation, and approximately a two-fold increase in ionic conductivity, reaching 13.99 mScm^{-1} at 25 °C. This also suggests that exploring the distinct behaviors and structure-function relationships associated with the electrolyte-electrode interfaces will be important directions for future applications.

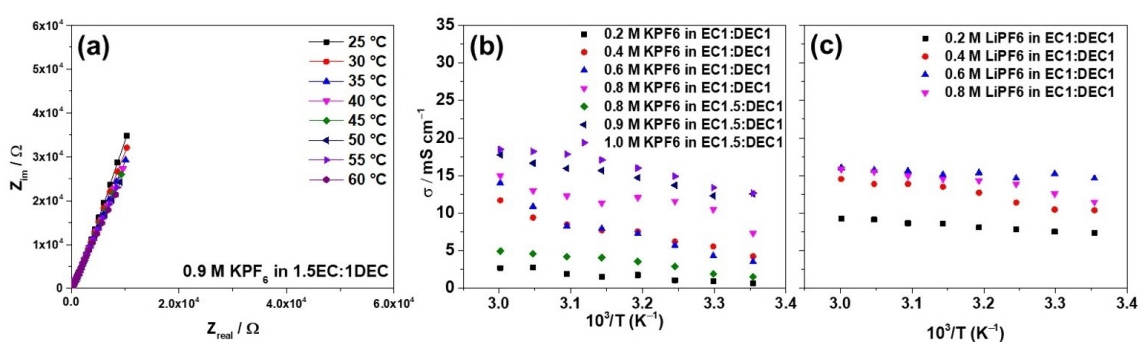


Figure 10. Electrochemical data at various temperatures: a) Nyquist plot of the 0.9 M KPF_6 in EC:DEC (ratio 1.5:1); b) ionic conductivities of potassium electrolytes; and c) ionic conductivities of lithium electrolytes in EC:DEC (ratio 1.5:1) for comparison.

Acknowledgements

J.R. was supported by CONACYT-SENER project No. 274314. Author would like to thanks to National Science Foundation for supporting potassium ion battery safety work under the CBET-1804300 grant and U.S. Office of Naval Research (ONR, N00014-16-1-2465) for lithium ion electrolyte work.

Conflict of Interest

The authors declare no conflict of interest.

Keywords: K- and Li-ion electrolytes • ionic conductivity • solubility • solvation shell structure

- [1] A. Yoshino, Development of the Lithium-Ion Battery and Recent Technological Trends, Elsevier, 2014.
- [2] B. Dunn, H. Kamath, J.-M. Tarascon, *Science* **2011**, *334*, 928.
- [3] N. Yabuuchi, K. Kubota, M. Dahbi, S. Komaba, *Chem. Rev.* **2014**, *114*, 11636.
- [4] K. Kubota, M. Dahbi, T. Hosaka, S. Kumakura, S. Komaba, *Chem. Rec.* **2018**, *18*, 459.
- [5] A. A. Yaroshevsky, *Geochem. Int.* **2006**, *44*, 48.
- [6] T. Hosaka, K. Kubota, A. S. Hameed, S. Komaba, *Chem. Rev.* **2020**, *120*, 6358.
- [7] N. Xiao, W. D. McCulloch, Y. Wu, *J. Am. Chem. Soc.* **2017**, *139*, 9475.
- [8] P. Bhariyal, A. Mahata, B. Pathak, *J. Phys. Chem. C* **2018**, *122*, 2481.
- [9] J. C. Pramudita, D. Sehrawat, D. Goonetilleke, N. Sharma, *Adv. Energy Mater.* **2017**, *7*, 1.
- [10] B. Ji, F. Zhang, N. Wu, Y. Tang, *Adv. Energy Mater.* **2017**, *7*, 1.
- [11] L. Jiang, Y. Lu, C. Zhao, L. Liu, J. Zhang, Q. Zhang, X. Shen, J. Zhao, X. Yu, H. Li, X. Huang, L. Chen, Y. S. Hu, *Nat. Energy* **2019**, *4*, 495.
- [12] B. Huang, Y. Shao, Y. Liu, Z. Lu, X. Lu, S. Liao, *ACS Appl. Energ. Mater.* **2019**, *2*, 6528.
- [13] J. Han, G. N. Li, F. Liu, M. Wang, Y. Zhang, L. Hu, C. Dai, M. Xu, *Chem. Commun.* **2017**, *53*, 1805.
- [14] Y. Hu, W. Tang, Q. Yu, X. Wang, W. Liu, J. Hu, C. Fan, *Adv. Funct. Mater.* **2020**, *30*, 2000675.
- [15] S. Liu, M. Xiong, W. Tang, Y. Hu, Y. Yan, L. Xu, C. Fan, *ACS Appl. Mater. Interfaces* **2021**, *13*, 38315.

- [16] L. Zhou, Z. Cao, W. Wahyudi, J. Zhang, J. Y. Hwang, Y. Cheng, L. Wang, L. Cavallo, T. Anthopoulos, Y. K. Sun, H. N. Alshareef, J. Ming, *ACS Energy Lett.* **2020**, *5*, 766.
- [17] W. Zhang, Y. Liu, Z. Guo, *Sci. Adv.* **2019**, *5*, 1.
- [18] R. Rajagopalan, Y. Tang, X. Ji, C. Jia, H. Wang, *Adv. Funct. Mater.* **2020**, *30*, 1.
- [19] J. Xie, J. Li, W. Zhuo, W. Mai, *Mater. Today* **2020**, *6*, 100035.
- [20] S. Liu, J. Mao, Q. Zhang, Z. Wang, W. K. Pang, L. Zhang, A. Du, V. Sencadas, W. Zhang, Z. Guo, *Angew. Chem. Int. Ed.* **2020**, *59*, 3638.
- [21] L. Deng, L. Deng, T. Wang, Y. Hong, M. Feng, R. Wang, J. Zhang, Q. Zhang, J. Wang, L. Zeng, Y. Zhu, Y. Zhu, L. Guo, *ACS Energy Lett.* **2020**, *5*, 1916.
- [22] B. Li, J. Zhao, Z. Zhang, C. Zhao, P. Sun, P. Bai, J. Yang, Z. Zhou, Y. Xu, *Adv. Funct. Mater.* **2019**, *29*, 1.
- [23] H. Wang, D. Yu, X. Wang, Z. Niu, M. Chen, L. Cheng, W. Zhou, L. Guo, *Angew. Chem. Int. Ed.* **2019**, *58*, 16451.
- [24] T. A. Pham, K. E. Kweon, A. Samanta, V. Lordi, J. E. Pask, *J. Phys. Chem. C* **2017**, *121*, 21913.
- [25] R. A. Adams, A. Varma, V. G. Pol, *Adv. Energy Mater.* **2019**, *9*, 1900550.
- [26] M. G. Giorgini, K. Futamatagawa, H. Torii, M. Musso, S. Cerini, *J. Phys. Chem. Lett.* **2015**, *6*, 3296.
- [27] J. E. Katon, M. D. Cohen, *Can. J. Chem.* **1975**, *53*, 1378.
- [28] D. M. Seo, S. Reininger, M. Kutcher, K. Redmond, W. B. Euler, B. L. Lucht, *J. Phys. Chem. C* **2015**, *119*, 14038.
- [29] S. I. Lee, U. H. Jung, Y. S. Kim, M. H. Kim, D. J. Ahn, H. S. Chun, *Korean J. Chem. Eng.* **2002**, *19*, 638.
- [30] B. Ravikumar, M. Mynam, B. Rai, *J. Phys. Chem. C* **2018**, *122*, 8173.
- [31] L. D. Kock, M. D. S. Lekgoathi, P. L. Crouse, B. M. Vilakazi, *J. Mol. Struct.* **2012**, *1026*, 145.
- [32] K. D. Fulfer, D. G. Kuroda, *J. Phys. Chem. C* **2016**, *120*, 24011.
- [33] M. Nie, D. P. Abraham, D. M. Seo, Y. Chen, A. Bose, B. L. Lucht, *J. Phys. Chem. C* **2013**, *117*, 25381.
- [34] F. Wang, F. Varenne, D. Ortiz, V. Pinzio, M. Mostafavi, S. Le Caer, *ChemPhysChem* **2017**, *18*, 2799.
- [35] N. Chapman, O. Borodin, T. Yoon, C. C. Nguyen, B. L. Lucht, *J. Phys. Chem. C* **2017**, *121*, 2135.
- [36] D. Frenkel, B. Smit, Understanding Molecular Simulation: From Algorithms to Applications, Elsevier, 2002.
- [37] M. C. Turk, C. A. Johnson, D. Roy, *J. Energy Storage* **2018**, *20*, 395.
- [38] J. Hwang, K. Matsumoto, R. Hagiwara, *J. Phys. Chem. C* **2018**, *122*, 26857.

Manuscript received: August 19, 2021

Revised manuscript received: September 21, 2021

Version of record online: October 18, 2021